



## Influence of Synaptic Vesicle Position on Release Probability and Exocytotic Fusion Mode

Hyocheon Park *et al.*

*Science* **335**, 1362 (2012);

DOI: 10.1126/science.1216937

*This copy is for your personal, non-commercial use only.*

If you wish to distribute this article to others, you can order high-quality copies for your colleagues, clients, or customers by [clicking here](#).

Permission to republish or repurpose articles or portions of articles can be obtained by following the guidelines [here](#).

**The following resources related to this article are available online at [www.sciencemag.org](http://www.sciencemag.org) (this information is current as of July 15, 2013):**

**Updated information and services**, including high-resolution figures, can be found in the online version of this article at:

<http://www.sciencemag.org/content/335/6074/1362.full.html>

**Supporting Online Material** can be found at:

<http://www.sciencemag.org/content/suppl/2012/02/15/science.1216937.DC1.html>

A list of selected additional articles on the Science Web sites **related to this article** can be found at:

<http://www.sciencemag.org/content/335/6074/1362.full.html#related>

This article **cites 35 articles**, 12 of which can be accessed free:

<http://www.sciencemag.org/content/335/6074/1362.full.html#ref-list-1>

This article has been **cited by 5 articles** hosted by HighWire Press; see:

<http://www.sciencemag.org/content/335/6074/1362.full.html#related-urls>

This article appears in the following **subject collections**:

Cell Biology

[http://www.sciencemag.org/cgi/collection/cell\\_biol](http://www.sciencemag.org/cgi/collection/cell_biol)

force on the ER membrane to overcome the membrane-bending energy of this asymmetric membrane. We deleted the flexible region that links the ACE and  $\beta$ -propeller domains of Sec31p, creating an edge element that might be expected to exhibit structural rigidity conferred by direct apposition of the two domains (Fig. 4A). Indeed, the corresponding mutant, *sec31- $\Delta$ hinge*, supported viability independent of a *bst* mutation (Fig. 4B). In contrast, deletion of the DIM alone, which preserves a short flexible domain and a disordered loop missing from the crystal structure, did not suffice for viability unless an additional *bst* mutation was present (*sec31- $\Delta$ blade* in Fig. 4B). The purified Sec31p- $\Delta$ hinge protein assembled on synthetic liposomes (Fig. 4C), suggesting robust functionality. In cells expressing only this rigidified form of Sec31p, Sec13p-GFP redistributed from large ER exit sites to a diffuse cytosolic localization with a coincident increase in nuclear envelope fluorescence (Fig. 4D). Small residual puncta may have reflected a Sec16p-associated pool of Sec13p (7), which is not required for viability because, unexpectedly, *SEC13* could be deleted entirely when Sec31p- $\Delta$ hinge was expressed (Fig. 4E). ER exit sites, as marked by Sec24p-GFP, were normal in *sec31- $\Delta$ hinge* mutant cells that lacked Sec13p (Fig. 4D), and secretory protein maturation *in vivo* was indistinguishable from wild-type cells (Fig. 4F), suggesting that ER export was fully operational in the absence of Sec13p. We tested the effect of converse mutations in Sec31p—those that might decrease rigidity of the Sec13/31p complex by destabilizing the  $\beta$ -propeller interface—and demonstrated that one such mutant was viable only in a *sec31 $\Delta$ emp24 $\Delta$*  background, despite being able to assemble into a Sec13/31p complex (fig. S8). We thus propose that Sec13p rigidifies the COPII cage, increasing its membrane-bending capacity; when a *bst* mutation creates a donor membrane more permissive to deformation, this function of Sec13p is no longer required (fig. S7).

By exploiting the *bst* phenotype to understand how secretion occurs when the COPII coat is compromised, we determined that cargo sorting can impact vesicle formation. We propose that *bst* mutations create a locally altered membrane that lacks the full complement of asymmetrically distributed cargo proteins such that the membrane can be deformed into a small vesicle absent the rigidifying effect of Sec13p. Indeed, a truncated form of Sec31p that lacks a flexible domain encompassing the Sec13p interaction motif supports viability in the absence of a *bst* mutation, suggesting that an artificially rigidified coat can exert sufficient force to bend an asymmetric cargo-rich membrane. Membrane-bending properties of coat proteins have largely been characterized on synthetic liposomes (23–25), which fail to recapitulate important properties of cellular membranes, including the abundance and complexity of protein cargoes and the asymmetry that lipids and proteins can exhibit across the bilayer. Coat proteins have evolved to overcome

the barrier to curvature that such constituents present, employing multiple mechanisms to enforce shape changes (4). The structural rigidity conferred to the COPII coat by Sec13 has parallels in other vesicle transport systems, notably the clathrin coat, where structural models predict that depletion of clathrin light chain renders the heavy-chain triskelion more flexible, yet still competent for vesicle formation (26). The presence of Sec13 within the COPII cage may also permit multiple geometries, allowing the coat to adapt to cell- or condition-specific cargo packaging requirements (27). Indeed, mammalian cells depleted of Sec13 show collagen-specific trafficking defects (28) that may reflect the inability of a Sec13-free coat to adequately deform the membrane around a uniquely rigid cargo. Furthermore, ER export of large cargoes requires alternative COPII subunits like the yeast Sec24p paralog Lst1p/Sfb2p, which facilitates traffic of the abundant oligomeric Pma1p complex (29, 30), or accessory factors such as human TANGO1, which promotes trafficking of procollagen (31). Such accessory proteins could influence membrane properties to either oppose the force of the COPII coat, preventing premature vesicle scission, or augment curvature conferred by the coat to ensure encapsulation of a rigid cargo. In addition to large and rigid cargoes, we propose that proteins with particularly asymmetric topologies will also influence the mechanics of vesicle formation.

#### References and Notes

1. E. A. Miller, C. Barlowe, *Curr. Opin. Cell Biol.* **22**, 447 (2010).
2. X. Bi, R. A. Corpina, J. Goldberg, *Nature* **419**, 271 (2002).
3. S. M. Stagg *et al.*, *Nature* **439**, 234 (2006).
4. J. Zimmerberg, M. M. Kozlov, *Nat. Rev. Mol. Cell Biol.* **7**, 9 (2006).
5. S. Fath, J. D. Mancias, X. Bi, J. Goldberg, *Cell* **129**, 1325 (2007).
6. S. G. Brohawn, T. U. Schwartz, *Nat. Struct. Mol. Biol.* **16**, 1173 (2009).
7. J. R. R. Whittle, T. U. Schwartz, *J. Cell Biol.* **190**, 347 (2010).
8. M. J. Elrod-Erickson, C. A. Kaiser, *Mol. Biol. Cell* **7**, 1043 (1996).

9. M. Marzoch *et al.*, *Mol. Biol. Cell* **10**, 1923 (1999).
10. Materials and methods are available as supporting material on Science Online.
11. C. Barlowe *et al.*, *Cell* **77**, 895 (1994).
12. A. H. Tong *et al.*, *Science* **294**, 2364 (2001).
13. M. Fujita, Y. Jigami, *Biochim. Biophys. Acta* **1780**, 410 (2008).
14. M. Fujita *et al.*, *Cell* **139**, 352 (2009).
15. M. Muñiz, C. Nuooffer, H. P. Hauri, H. Riezman, *J. Cell Biol.* **148**, 925 (2000).
16. M. Fujita *et al.*, *J. Cell Biol.* **194**, 61 (2011).
17. A. Copic *et al.*, *Genetics* **182**, 757 (2009).
18. W. J. Belden, C. Barlowe, *Science* **294**, 1528 (2001).
19. J. Dancourt, C. Barlowe, *Annu. Rev. Biochem.* **79**, 777 (2010).
20. S. Ghaemmaghami *et al.*, *Nature* **425**, 737 (2003).
21. G. K. Voeltz, W. A. Prinz, Y. Shibata, J. M. Rist, T. A. Rapoport, *Cell* **124**, 573 (2006).
22. R. Schneider *et al.*, *Biochem. J.* **381**, 941 (2004).
23. M. C. S. Lee *et al.*, *Cell* **122**, 605 (2005).
24. A. Bielli *et al.*, *J. Cell Biol.* **171**, 919 (2005).
25. B. J. Peter *et al.*, *Science* **303**, 495 (2004).
26. J. D. Wilbur *et al.*, *Dev. Cell* **18**, 854 (2010).
27. S. M. Stagg *et al.*, *Cell* **134**, 474 (2008).
28. A. K. Townley *et al.*, *J. Cell Sci.* **121**, 3025 (2008).
29. K. J. Roberg, M. Crotwell, P. Espenshade, R. Gimeno, C. A. Kaiser, *J. Cell Biol.* **145**, 659 (1999).
30. Y. Shimoni *et al.*, *J. Cell Biol.* **151**, 973 (2000).
31. K. Saito *et al.*, *Cell* **136**, 891 (2009).

**Acknowledgments:** We thank J. Goldberg, C. Boone, E. Snapp, and M. Lee for strains and reagents; T. Swayne, E. Bauer, R. Rothstein, J. Dittmar, and members of the Rothstein laboratory for technical assistance; and B. Antonny, J. Derganc, M. Lee, and F. Pincet for valuable discussions. This work was supported by a Columbia Research Initiatives in Science and Engineering award and NIH grants GM085089 and GM078186 to E.A.M. and by a Columbia Frontiers of Science fellowship to A.C. M.A.H. was an I. I. Rabi Science Scholar of Columbia University. Additional data described in the manuscript are presented in the supporting online material.

#### Supporting Online Material

www.sciencemag.org/cgi/content/full/science.1215909/DC1  
Materials and Methods  
Figs. S1 to S8  
Tables S1 and S2  
References (32–42)

28 October 2011; accepted 20 January 2012  
Published online 2 February 2012;  
10.1126/science.1215909

## Influence of Synaptic Vesicle Position on Release Probability and Exocytotic Fusion Mode

Hyocheon Park,<sup>1</sup> Yulong Li,<sup>1</sup> Richard W. Tsien<sup>1,2\*</sup>

Neurotransmission depends on movements of transmitter-laden synaptic vesicles, but accurate, nanometer-scale monitoring of vesicle dynamics in presynaptic terminals has remained elusive. Here, we report three-dimensional, real-time tracking of quantum dot-loaded single synaptic vesicles with an accuracy of 20 to 30 nanometers, less than a vesicle diameter. Determination of the time, position, and mode of fusion, aided by trypan blue quenching of Qdot fluorescence, revealed that vesicles starting close to their ultimate fusion sites tended to fuse earlier than those positioned farther away. The mode of fusion depended on the prior motion of vesicles, with long-dwelling vesicles preferring kiss-and-run rather than full-collapse fusion. Kiss-and-run fusion events were concentrated near the center of the synapse, whereas full-collapse fusion events were broadly spread.

Neurons communicate by releasing neurotransmitter and thus activating postsynaptic receptors. The position and movement

of neurotransmitter-containing vesicles are essential for proper communication. However, vesicle dynamics during the period leading up to release

remain mysterious. Uncertainty exists about the possible role of vesicle position in the determination of vesicle fusion probability (*I*). A controversy concerns the possible existence of two modes of fusion—full-collapse fusion (FCF) or kiss-and-run (K&R)—reported in central nervous system (CNS) neurons (2–6), but having an uncertain relation between vesicle movement and fusion location—especially in three dimensions (7). Recently, several methods have been devel-

oped to localize fluorescent molecules in three dimensions (8–10) but real-time three-dimensional (3D) localization has not been applied to synaptic vesicles in living neurons.

To localize single synaptic vesicles in real-time and in three dimensions, we built a microscope with dual-focus imaging optics, modified from a published design (9) (fig. S1). The accuracy of the localization ( $2.35 \sigma$ , corresponding to the full-width at half maximum) was  $\sim 20$  nm for *x*- and *y*- and  $\sim 30$  nm for *z*-localization (Fig. 1A) (for 10 Hz imaging, standard in this paper). Real-time capabilities were tested by imposing stepwise movements on single Qdot-containing vesicles in a fixed neuron. For *z* axis displacements of 40 nm ( $\sim 1$  vesicle diameter), the estimated *z* axis displacement for individual frames was  $42 \pm 2.7$  nm (SEM)

(*n* = 10) (Fig. 1B), an accuracy well below a single vesicle diameter.

Single vesicles were efficiently labeled by use of streptavidin-coated Qdots conjugated to biotinylated antibodies against the luminal domain of the vesicular protein synaptotagmin 1. In an exemplar 3D trajectory (Fig. 1C), a single vesicle in a living neuron underwent  $\sim 12$  s of intense movement, travelling almost unidirectionally with the net displacement of  $3.2 \mu\text{m}$  over 90 s of imaging, with dwelling in two discrete zones, presumptive presynaptic terminals marked by distinct clouds of vesicles labeled with FM 4-64, a lipophilic probe for vesicular turnover.

Exocytosis of the Qdot-loaded vesicles was registered by a sudden drop in the fluorescence, caused by uptake of an extracellular quencher,

<sup>1</sup>Department of Molecular and Cellular Physiology, Stanford University, Stanford, CA 94305, USA. <sup>2</sup>NYU Neuroscience Institute and Department of Physiology and Neuroscience, New York University, New York, NY 10016, USA.

\*To whom correspondence should be addressed. E-mail: richard.tsien@nyumc.org

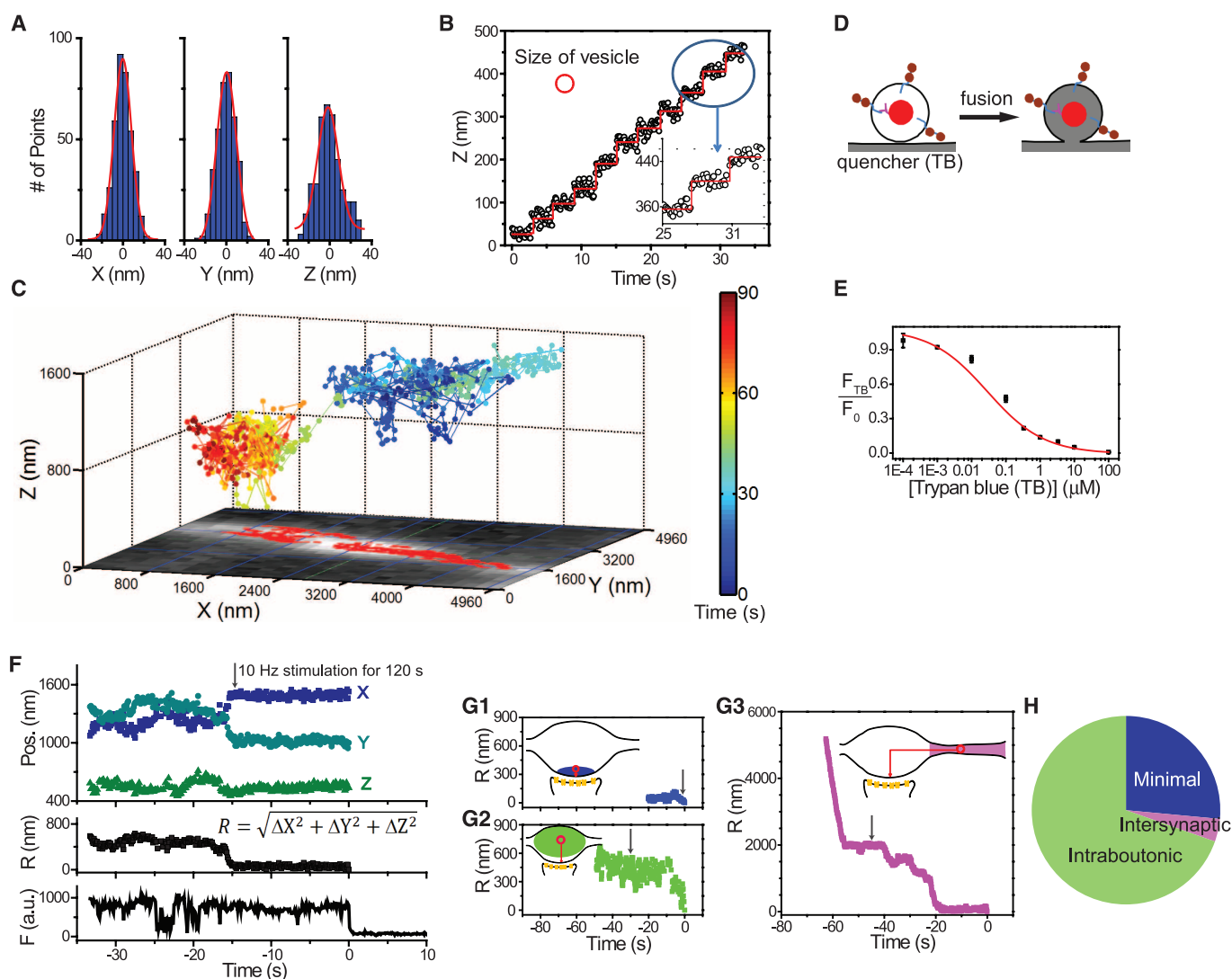


**Fig. 1.** Real-time, 3D tracking of single vesicles. (A) Immobilized Qdot (10-Hz imaging). Positional estimates had standard deviations ( $\sigma$ ) of 8.5 nm (*x*), 8.5 nm (*y*), and 12.3 nm (*z*). (B) Tracking *z*-axial, 40-nm movements of a single Qdot in a fixed neuron. Red circle, approximate size of a vesicle. (Inset) Expanded view. (C) 3D trace of Qdot-labeled vesicle in living neuron, with *x-y* plane projection (red squares), overlaid on image of FM 4-64-labeled vesicles (white). Color bar, elapsed time. Stimulation (10 Hz, 120 s) started at 20 s; vesicle exocytosed at 90 s.

(D) Quenching of Qdot fluorescence by TB pinpoints the moment of exocytosis. (E) Dependence of unquenched fraction ( $F_{TB}/F_0$ ) on TB concentration. (F) 3D position and fluorescence of Qdot-labeled vesicle (exocytosis,  $t = 0$ ). (G) Traces and representations of minimal, intraboutonic, and intersynaptic patterns of vesicle movement before exocytosis (G1 to G3, respectively). Average latencies to fusion were 40.7, 42.9, and 55.5 s, respectively. Gray arrows, initiation of 1200 APs stimulation. (H) Prevalence of three patterns of movement.

trypan blue (TB) (6, 11) (Fig. 1D). We used 1  $\mu\text{M}$  TB in most experiments, guided by the concentration dependence of TB quenching of Qdots ( $F_{\text{TB}}/F_0$ ) (Fig. 1E). Neither the quencher nor loading with antibody-conjugated Qdots affected vesicle dynamics, as assessed by uptake and destaining of FM 4-64 (fig. S2).

We analyzed 3D positions over time, calculating the momentary radial distance to the eventual location of fusion ( $R = \sqrt{\Delta X^2 + \Delta Y^2 + \Delta Z^2}$ ). In one example (Fig. 1F), a tracked vesicle was mo-

bile for the first 18 s of imaging but then remained stationary at the fusion site ( $R \approx 0$ ) for another 15 s before undergoing fusion ( $t=0$ ). The fluorescence trace included a blinking event ( $-24$  s), which confirmed that the signal arose from a single Qdot, and displayed a sharp drop 14 s after the onset of field stimulation, which corresponded to complete equilibration of the vesicle lumen with the quencher-containing external solution. Similar traces were obtained from  $\gamma$ -aminobutyric acid (GABA)-releasing (GABAergic) terminals, by

using Qdots conjugated to biotinylated antibodies against the luminal domain of vesicular GABA transporter (VGAT) (fig. S3A).

Single vesicles displayed three patterns of movement before exocytosis—intersynaptic, intraboutonic, and minimal (residing very close to the fusion site for the entire observation period). Intersynaptic movement was categorized by a net displacement of  $>1 \mu\text{m}$  (Fig. 1, C and G3), consistent with vesicle sharing between nearby synapses (12), and was the least prevalent [3 out of 81 (4%)] (Fig. 1H). Intraboutonic movement, defined by net displacements between  $0.1 \mu\text{m}$  and  $1 \mu\text{m}$  (Fig. 1G2), was the most abundant pattern [56 out of 81 (69%)], presumably because it typifies the bulk of recycling vesicles. Net movements of  $<0.1 \mu\text{m}$  before exocytosis (Fig. 1G1), categorized as minimal, were observed in 22 of 81 (27%) of cases.

Next, we tested whether proximity to release sites is a critical determinant of vesicle-release probability (Fig. 2). This long-held assumption (1, 13) predicts that, on average, a vesicle starting off close to its ultimate release site will fuse earlier than one located further away. Accordingly, we directly determined the net 3D displacement from the starting position of vesicles to their fusion sites, information unobtainable from static electron microscopy (EM) images. The net displacement to fusion site proved to be a strong predictor of the latency to fusion ( $P < 0.005$ ) (fig. S4). Vesicles with relatively high release probability (high  $P_{\text{TV}}$ ) were defined by a brief latency to release ( $<20$  s after onset of stimulation), whereas vesicles with relatively low  $P_{\text{TV}}$  were discerned by long latency ( $>50$  s after onset of

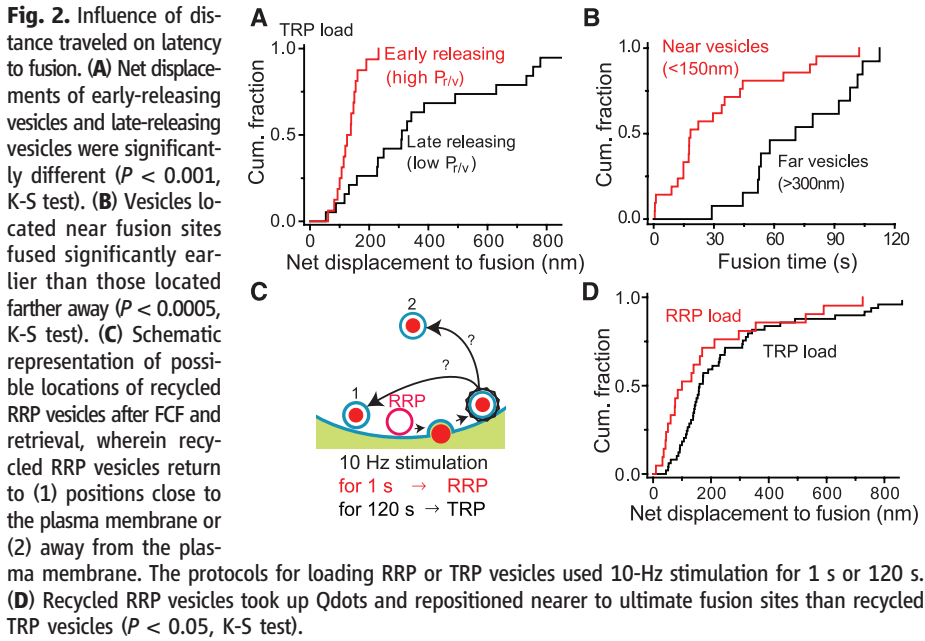
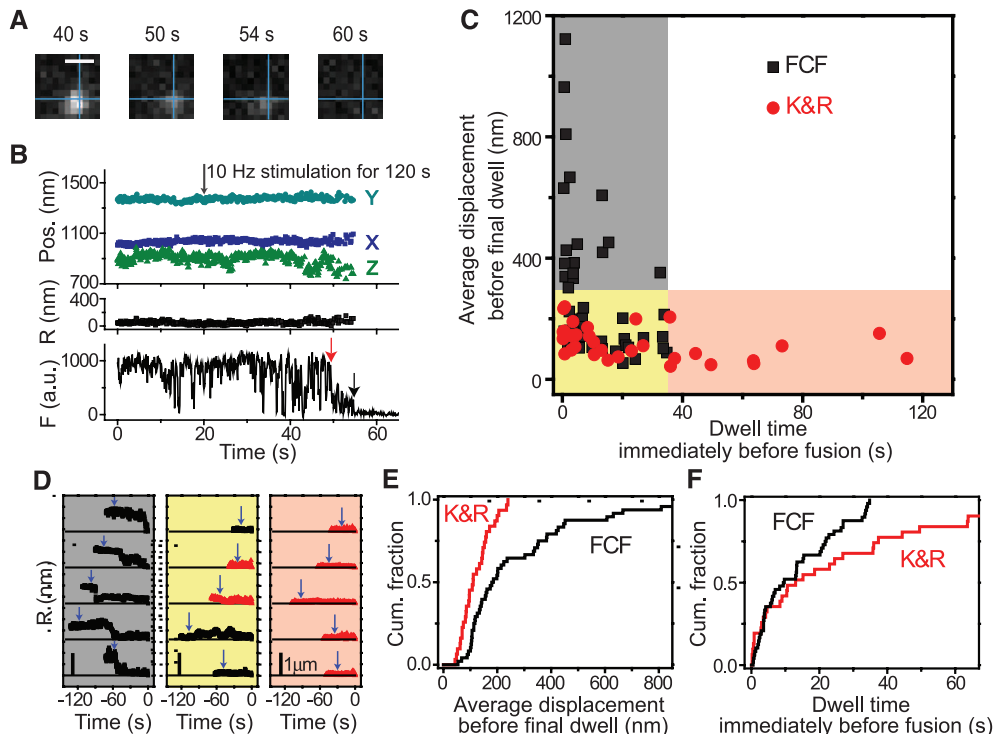


**Fig. 3.** Detection of K&R by partial quenching and relation of fusion mode to prior motion. (A) Images taken before fusion (40 s), after partial quenching (50 s), and before (54 s) and after full quenching (60 s). The intersection of the perpendicular lines marked the position before the first fusion. Bar,  $0.8 \mu\text{m}$ . (B) 3D position and fluorescence of Qdot-loaded vesicle in (A). Red arrow, K&R; black arrow, final FCF event. (C) Relation of fusion mode to final dwell time and average displacement preceding final dwell. (D) Traces exemplifying three categorized groups. Blue arrows, stimulation initiation. Bar,  $1 \mu\text{m}$ . (E) Average displacements before final dwell were significantly smaller with K&R (average,  $105 \pm 10.8 \text{ nm}$ ,  $n = 22$ ) than with FCF (average,  $278 \pm 34.2 \text{ nm}$ ,  $n = 48$ ) ( $P < 0.005$ , K-S test). (F) Dwell times at the final position were significantly longer with K&R (average,  $30.3 \pm 7.01 \text{ s}$ ) than with FCF (average,  $10.7 \pm 1.55 \text{ s}$ ) ( $P < 0.001$ , K-S test).



stimulation). The high  $P_{r/v}$  vesicles traveled a shorter distance to fusion sites (median, 125 nm,  $n = 15$ ) than low  $P_{r/v}$  vesicles (median, 310 nm,  $n = 19$ ) [ $P < 0.001$ , Kolmogorov–Smirnov (K-S) test] (Fig. 2A). Likewise, vesicles starting near fusion sites ( $<150$  nm) underwent exocytosis earlier (median, 18 s; average,  $31 \pm 6.2$  s;  $n = 21$ ) than those starting further away ( $>300$  nm) (median, 71 s; average,  $73 \pm 7.4$  s;  $n = 13$ ) ( $P < 0.0005$ , K-S test) (Fig. 2B). Thus, proximity is a key factor in determining vesicle release probability even for vesicles not already docked to their release site.

To determine whether a vesicle's pool of origin influences its eventual position after FCF and retrieval or if vesicles become randomly dispersed (Fig. 2C), we investigated the positions of the readily releasable pool (RRP) and total recycling pool (TRP) of vesicles after recycling, in experiments akin to those in previous EM studies (14, 15). Labeling of vesicles was either sharply restricted to vesicles from the RRP {10 Hz for 1 s [10 action potential (AP) stimulation]} or spread across the TRP (1200 APs). Vesicles originating from the RRP relocated at positions significantly closer to the fusion sites (median 100 nm,  $n = 21$ ) (Fig. 2D) than vesicles derived from the TRP (median 160 nm,  $n = 49$ )

(K-S test,  $P < 0.05$ ) [see also (15)]. The observed difference in spatial distribution was remarkable, because Qdots (unlike FM dye) can only be taken up after FCF and clathrin-mediated retrieval (Fig. 2C) (5). Nevertheless, vesicles with a high probability of release in a first round of exocytosis behaved detectably differently compared with recycling vesicles as a whole, consistent with a role for molecular determinants as contributors to pool identity (14). Such determinants may apply to RRP vesicles that reside far enough from the fusion site to be strictly undocked (1, 13, 14).

The degree of quenching of Qdot fluorescence by TB distinguished FCF and K&R. TB should completely equilibrate after FCF but only partially equilibrate during a brief fusion pore opening of K&R. Partial quenching of a single Qdot due to K&R is illustrated in Fig. 3A (see detailed analyses in SOM and fig. S5). The fluorescence trace showed a sudden, irreversible, but only partial, drop (red arrow), falling from an initial level (defined as 1.0) to a partially quenched level ( $F_{TB}/F_0 = 0.312$ ), significantly larger than expected for Qdots steadily exposed to 1  $\mu\text{M}$  TB [ $0.137 \pm 0.003$  (SEM),  $n = 3$ ]. After a sojourn of  $\sim 5$  s, the fluorescence dropped further (black arrow), to a level of virtually zero, presumably in association with Qdot movement out of the region

of interest after full fusion. Similar two-step losses of fluorescence, apparently K&R and FCF events in succession, were observed with single vesicles in inhibitory nerve terminals, tracked with VGAT-antibody-conjugated Qdots (fig. S3B). We verified that partial quenching denoted K&R fusion by using a lower quencher concentration and observing a milder degree of partial quenching (fig. S6A).

On many occasions, the Qdot-labeled vesicle remained stationary before undergoing K&R (Fig. 3B), which raised the question of whether the fusion mode is influenced by prior motion. To investigate this, we determined the final dwell time before fusion and the average displacement before that final dwell. These parameters varied between the two fusion modes (Fig. 3C; specific examples in Fig. 3D). Vesicles located close ( $<300$  nm) to their fusion sites with dwell times longer than 35 s (pink shading) invariably underwent K&R. In contrast, vesicles that approached from a long distance ( $>300$  nm) before the final dwell time (gray shading) consistently underwent FCF. Vesicles characterized by both a brief dwell time and previously close proximity to fusion sites showed mixed results (yellow shading). Analysis of pooled data (Fig. 3, E and F) confirmed that vesicles undergoing K&R traveled shorter distances to reach fusion sites than those undergoing FCF ( $P < 0.005$ , K-S test), whereas vesicles undergoing K&R remained stationary at fusion sites for longer than those undergoing FCF ( $P < 0.001$ , K-S test). Thus, determination of fusion mode is not a strictly stochastic decision at the time of exocytosis but is strongly dependent on the prior history of vesicle position.

Next, we pinpointed the locus of fusion relative to pre- and postsynaptic markers (Fig. 4, A and B): FM 4-64-stained presynaptic vesicles (red) and postsynaptic density protein PSD-95 fused to green fluorescent protein (PSD-95-GFP) (green). The “synaptic axis,” defined by a vector connecting centroids of pre- and postsynaptic markers ( $\rightarrow$ , Fig. 4, A and C), was presumed to pass roughly through the center of the active zone. The angle ( $\theta$ , Fig. 4A) between the synaptic axis and the  $z$  axis of the microscope was  $122^\circ$  in Fig. 4B (average,  $126 \pm 3.3^\circ$ ,  $n = 31$ ). The pre- and postsynaptic landmarks provided a spatial context for the pre-exocytosis motion of Qdot-labeled vesicles (Fig. 4C). The trajectory of an exemplar vesicle began near the center of FM 4-64 staining but ended at a site of exocytosis near the centroid labeled with PSD-95-GFP. Just before fusion by FCF (55.7 s) (black circle, Fig. 4C), the vesicle was 314 nm away from the synaptic axis ( $r = 314$  nm). Collectively, FCF events appeared evenly distributed over a disc centered on the synaptic axis, the cumulative distribution of events increasing with the square of distance ( $r^2$ ) (dashed line, Fig. 4D) [coefficient of determination ( $R^2$ ) = 0.94;  $r_{\text{median}} = 295$  nm;  $n = 22$ ]. In contrast, K&R events occurred closer to the synaptic axis ( $P < 0.001$ , K-S test), with  $r_{\text{median}} = 109$  nm, as if kept within a smaller zone ( $R^2 = 0.87$  for parabolic fit,  $n = 9$ ). The con-

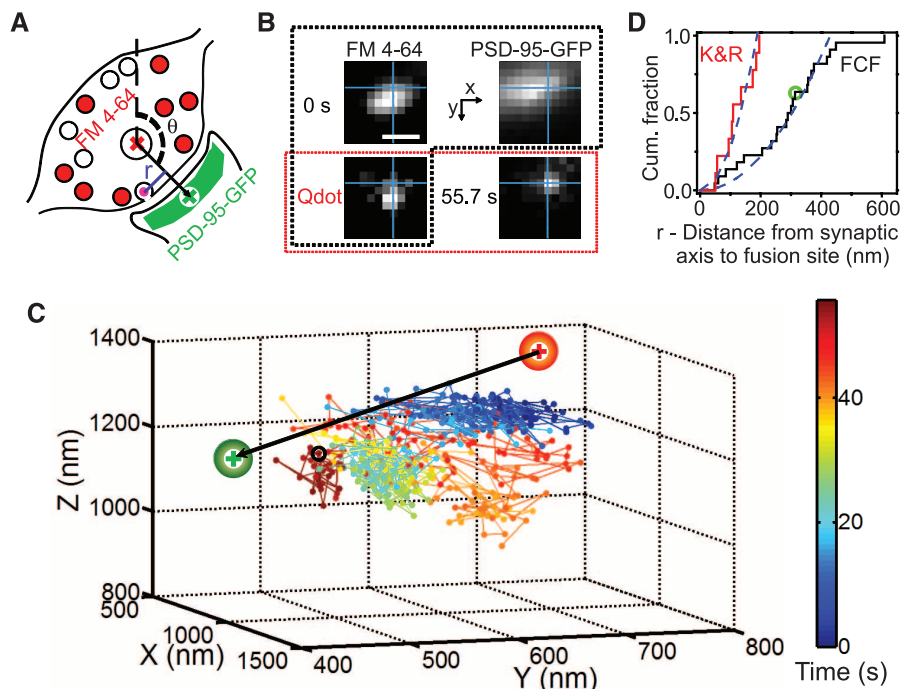


**Fig. 4.** Relation between fusion mode and proximity to synaptic axis ( $r$ ). (A) Synaptic axis ( $\rightarrow$ ) defined as a vector connecting centroids of FM 4-64 (+) and PSD-95-GFP (+), pre- and postsynaptic markers.  $r$  defined as orthogonal distance from fusion site to synaptic axis. (B) Images of FM 4-64, PSD-95-GFP, and Qdot in the same plane, taken initially (0 s, surrounded by dashed black line) and just before fusion (55.7 s). Images of Qdot are marked by a red-outlined rectangle. The intersection of the perpendicular lines marked the last position before fusion. Bar,  $0.8 \mu\text{m}$ . (C) 3D trajectory of the vesicle in (B) relative to FM 4-64 and PSD-95-GFP centroids. Color bar, elapsed time; 10-Hz stimulation starting at 20 s. Black circle, the last position before fusion. (D) Differing cumulative distributions of  $r$  for two fusion modes. Dashed line shows parabolic fit, corresponding to uniform distribution. Circle indicates the vesicle in Fig. 4, B and C.

finement of K&R events near the center of the presynaptic terminal would put glutamate release by K&R in alignment with *N*-methyl-D-aspartate receptors (NMDARs) located close to the center of the postsynaptic density but in less direct apposition with most of the fast  $\alpha$ -amino-3-hydroxy-5-methyl-4-isoxazolepropionic acid receptors (AMPA receptors), which appear dominant over NMDARs at the periphery (fig. S7) [(16, 17) but see also (18)]. Differences in alignment are important because (i) lateral spread of neurotransmitter causes rapid dilution of peak [glutamate] (19), with a lateral space constant of  $\sim 125$  nm (20) and (ii) AMPARs require millimolar [glutamate] for activation (21). Thus, our findings predict that exocytosis by K&R should strongly activate NMDARs but cause uneven activation of AMPARs, whereas both receptor types should be robustly activated by FCF, as recently found [(4), see also (22)].

Our real-time 3D tracking of single synaptic vesicles in living hippocampal nerve terminals enabled direct observation of the motion of single vesicles toward their fusion sites. It also revealed unexpected relations between the trajectory of vesicles, the location of fusion, and their mode of exocytosis.

## References and Notes

- S. O. Rizzoli, W. J. Betz, *Nat. Rev. Neurosci.* **6**, 57 (2005).
- A. M. Aravanis, J. L. Pyle, R. W. Tsien, *Nature* **423**, 643 (2003).
- S. P. Gandhi, C. F. Stevens, *Nature* **423**, 607 (2003).
- D. A. Richards, *J. Physiol.* **587**, 5073 (2009).
- Q. Zhang, Y. Li, R. W. Tsien, *Science* **323**, 1448 (2009).
- N. C. Harata, S. Choi, J. L. Pyle, A. M. Aravanis, R. W. Tsien, *Neuron* **49**, 243 (2006).
- P. Vanden Berghe, J. Klingauf, *J. Physiol.* **572**, 707 (2006).
- B. Huang, W. Wang, M. Bates, X. Zhuang, *Science* **319**, 810 (2008).
- T. M. Watanabe, T. Sato, K. Gonda, H. Higuchi, *Biochem. Biophys. Res. Commun.* **359**, 1 (2007).
- G. Shtengel *et al.*, *Proc. Natl. Acad. Sci. U.S.A.* **106**, 3125 (2009).
- M. Howarth *et al.*, *Nat. Methods* **5**, 397 (2008).
- K. J. Darcy, K. Staras, L. M. Collinson, Y. Goda, *Nat. Neurosci.* **9**, 315 (2006).
- A. Denker, S. O. Rizzoli, *Front. Synaptic Neurosci.* **2**, 135 (2010).
- S. O. Rizzoli, W. J. Betz, *Science* **303**, 2037 (2004).
- T. Schikorski, C. F. Stevens, *Nat. Neurosci.* **4**, 391 (2001).
- V. N. Kharazia, R. J. Weinberg, *Neurosci. Lett.* **238**, 41 (1997).
- P. Somogyi, Tamás, R. Lujan, E. H. Buhl, *Brain Res. Brain Res. Rev.* **26**, 113 (1998).
- A. Dani, B. Huang, J. Bergan, C. Dulac, X. Zhuang, *Neuron* **68**, 843 (2010).
- V. V. Uteshev, P. S. Pennefather, *Biophys. J.* **72**, 1127 (1997).
- K. M. Franks, C. F. Stevens, T. J. Sejnowski, *J. Neurosci.* **23**, 3186 (2003).
- J. S. Diamond, C. E. Jahr, *J. Neurosci.* **17**, 4672 (1997).
- S. Choi, J. Klingauf, R. W. Tsien, *Philos. Trans. R. Soc. London B Biol. Sci.* **358**, 695 (2003).

**Acknowledgments:** We thank Q. Zhang for discussion and for first applying Qdots to the research on vesicle release; T. Watanabe for help with building the 3D microscope; S. Syed, S.-Y. Oh, and S. Ryu for analysis programs; I. Shim for help with data analysis; A. Mitra for the construct for PSD-95-GFP; H. Martens for biotinylated antibodies against VGAT; and members of the Tsien lab for discussion. Supported by grants from National Institute of Mental Health (NIH), the Burnett Family Foundation, and Mathers Foundation.

## Supporting Online Material

www.sciencemag.org/cgi/content/full/science.1216937/DC1  
Materials and Methods  
SOM Text  
Figs. S1 to S9  
References (23–35)

21 November 2011; accepted 31 January 2012  
Published online 16 February 2012;  
10.1126/science.1216937

# Decoding in the Absence of a Codon by tmRNA and SmpB in the Ribosome

Cajetan Neubauer,<sup>1\*</sup> Reynald Gillet,<sup>2</sup> Ann C. Kelley,<sup>1</sup> V. Ramakrishnan<sup>1†</sup>

In bacteria, ribosomes stalled at the end of truncated messages are rescued by transfer-messenger RNA (tmRNA), a bifunctional molecule that acts as both a transfer RNA (tRNA) and a messenger RNA (mRNA), and SmpB, a small protein that works in concert with tmRNA. Here, we present the crystal structure of a tmRNA fragment, SmpB and elongation factor Tu bound to the ribosome at 3.2 angstroms resolution. The structure shows how SmpB plays the role of both the anticodon loop of tRNA and portions of mRNA to facilitate decoding in the absence of an mRNA codon in the A site of the ribosome and explains why the tmRNA-SmpB system does not interfere with normal translation.

**T**ransfer-messenger RNA (tmRNA), also known as 10S RNA or SsrA, is a highly structured RNA that combines properties of transfer RNA (tRNA) and mRNA in one molecule about 350 nucleotides long (Fig. 1A) (1, 2). The tRNA-like domain (TLD) of tmRNA lacks an

anticodon stem loop but contains an acceptor arm (3) that can be aminoacylated at its 3' end by the same alanyl tRNA synthetase that aminoacylates tRNA<sup>Ala</sup>. A different region of tmRNA contains a short internal open reading frame (ORF) that acts as an mRNA template. In addition, tmRNA contains several pseudoknots and helices.

Ribosomes that reach the end of prematurely truncated or defective messages are stalled because the absence of a complete codon in the A site prevents either elongation or normal termination. In bacteria, they are rescued by tmRNA in a process called *trans*-translation because it involves continuing translation by changing the mRNA template. In this process, elongation factor Tu (EF-Tu) delivers tmRNA to the A site of

the stalled ribosome. The nascent polypeptide chain is transferred to the alanine on the TLD. Subsequently, translocation brings the first codon of the ORF into the A site of the ribosome, and translocation resumes with the ORF as the mRNA (2). The short sequence coded by the ORF thus added to the C terminus of the partially synthesized protein acts as a degradation tag (4). Therefore, tmRNA acts both to rescue ribosomes and to target incompletely synthesized proteins for degradation.

The binding of tmRNA to stalled ribosomes requires the protein SmpB (5), which can bind to tmRNA simultaneously with EF-Tu (6). Crystal structures of SmpB in complex with the TLD suggest that the protein substitutes for the missing anticodon stem inside the ribosome (7, 8), which was supported by electron microscopy (EM) studies at  $\sim 15$  Å resolution (9, 10). A previous EM study found two molecules of SmpB with tmRNA in the ribosome, with the C terminus of one of them near the decoding center of the 30S ribosomal subunit (11). The observed proximity to the decoding center agrees with hydroxyl radical and chemical probing experiments that show protection of 16S ribosomal RNA (rRNA) bases A1492, A1493, and G530 at the decoding center upon binding of the tmRNA-SmpB complex to the ribosome (*Escherichia coli* numbering used for rRNA throughout) (12, 13). However, mutations at these positions do not reduce SmpB binding to the decoding site (13) or reduce the rate of peptidyl transfer onto tmRNA (14). The mechanism by which tmRNA and SmpB acting in concert can facilitate “decoding” in the absence of codon-anticodon base pairing has remained unclear.

<sup>1</sup>Medical Research Council (MRC) Laboratory of Molecular Biology, Hills Road, Cambridge CB2 0QH, UK. <sup>2</sup>Université de Rennes 1 and Institut Universitaire de France, “Translation and Folding” group, UMR CNRS 6290, Institute of Genetics and Development of Rennes (IGDR), Campus de Beaulieu 35042 Rennes cedex, France.

\*Present address: Division of Geological and Planetary Sciences, California Institute of Technology, Pasadena, CA 91125, USA.

†To whom correspondence should be addressed. E-mail: ramak@mrc-lmb.cam.ac.uk